FURTHER RESULTS ON THE ZEROS OF A SLEWING RIGID-FLEXIBLE BEAM

Mohammad Vakil, Reza Fotouhi, Peter N. Nikiforuk
Mechanical Engineering Department, University of Saskatchewan
E-mail: m.vakil@usask.ca; reza.fotouhi@usask.ca; peter.nikiforuk@usask.ca

Received October 2009, Accepted November 2009
No. 09-CSME-65, E.I.C. Accession 3152

ABSTRACT

There is much research on the poles of the transfer function (between the beam-end displacement and base torque) of slewing single-flexible beams. However, there is no comprehensive report on their zeros. The study on the zeros is of great importance, especially from the controller design perspective, because some of these zeros are in the right-hand-side (RHS) of the domain S in the Laplace transform. These RHS zeros limit the control bandwidth; deteriorate the trade-off between the robustness and the desirable control performance. They also create challenges in the beam-end trajectory-tracking. It is for these reasons that a comprehensive study on the zeros is of valuable significance which for the first time is reported in this paper. It is shown here that the physical parameters of the slewing flexible beam fall into three categories with respect to the locations of the zeros. In the first category, an increase (or decrease) in values of physical parameters move the zeros further from (or closer to) the imaginary axis. The second category is composed of physical parameters where an increase (or decrease) in their values move the zeros closer to (or further from) the imaginary axis. The third category includes the physical parameters where the locations of the zeros are independent of their values.

Keywords: control; slewing flexible beam; non-minimum system; transfer function; zeros.

RÉSULTATS COMPLÉMENTAIRES SUR LES ZÉROS DANS UNE ROTATION D'UNE POUTRE RIGIDE-FLEXIBLE

RÉSUMÉ

Il ya beaucoup de recherches sur les pôles de la fonction de transfert (entre l'extrémité de la poutre et un couple de base) à rotation flexible pour poutre simple. Cependant, il n'existe pas de rapport détaillé sur leurs zéros. L'étude sur les zéros est de grande importance, surtout du point de vue de la conception du contrôleur. Parce que certains de ces zéros sont sur le côté droit (RHS) du domaine S dans la transformation de Laplace. Ces zéros RHS limite les fréquences de bande de pilotage; détériore le compromis entre la robustesse et la performance de régulation souhaitable. Ils créent aussi des défis pour traquer la trajectoire. C'est pour ces raisons qu'une étude approfondie sur les zéros est importante et que, pour la première fois, nous nous y intéressons dans ce document. Il est montré ici que les paramètres physiques de l'orientation de la poutre flexible se répartissent en trois catégories à l'égard de l'emplacement des zéros. Dans la première catégorie, une augmentation (ou réduction) des valeurs des paramètres physiques déplacer les zéros plus loin (ou plus proche) de l'axe imaginaire. La deuxième catégorie est composée de paramètres physiques où une augmentation (ou réduction) de leurs valeurs déplace les zéros plus proche (ou plus loin) de l'axe imaginaire. La troisième catégorie comprend les paramètres physiques où les emplacements des zéros sont indépendants de leurs valeurs.

Mots-clés : contrôle; rotation d'une poutre flexible; système de non-minimum; fonction de transfert; zéros.

1. INTRODUCTION

For a slewing single flexible beam, shown in Fig. 1, the transfer function between the base torque τ and the beam-end displacement y has right-hand-side (RHS) zeros in the domain S of the Laplace transform [1] and thus is a nonminimum phase system [2]. These RHS zeros are of critical importance as they limit the control bandwidth and deteriorate the trade-off between robustness and desirable control performance [3]. In addition, the RHS zeros create several challenges in the design of the beam-end trajectory-tracking controllers. Some of these challenges are (*i*)- non-causal beam-end inverse dynamic calculation [4] and (*ii*)- the dependency of the performance of the beam-end controllers on the location of the RHS zeros [5,(2 page 265),6,7,8,9]. Thus the study of the zeros is of great importance, which to the best of authors' knowledge has not been comprehensively reported so far.

To address the need for research on the zeros, an inclusive study on the zeros of a single flexible beam is performed here. For this purpose, a slewing single flexible beam with the initial part of the beam being rigid (SRFB), as shown in Fig. 2, is considered [10]. The reason for introducing and studying the zeros of a SRFB is that the precise modeling of an experimental setup, like the one in Fig. 3, requires that it be treated as a SRFB. The initial rigid section for this beam is because of the mounting brackets for measuring instruments.

To find the zeros of a SRFB, the authors' new theorem [11] which does not need deriving the transfer function between the beam-end displacement and the base input torque was used. Here, the phrase "zeros of SRFB" refers to the zeros of the transfer function of a SRFB considering the base torque as the input and beam-end displacement as the output. This theorem, which its proof is given in appendix I, states that:

Theorem: *The zeros of the transfer function of a slewing single rigid-flexible beam (SRFB), considering the torque at the base as the input and the displacement of the beam-end as the output, are the same as the zeros of the transfer function of the pinned-pinned beam counterpart of the SRFB, considering the torque at the base as the input and the shear force at the beam-end (other end) as the output.*

That is, the zeros of the transfer function $G = y(s)/\tau(s)$ in Fig. 2 are the same as the zeros of the transfer function $F = \upsilon(s)/\tau(s)$ in Fig. 4 where υ is the beam-end shear force. This new method, which has been mathematically proven in appendix I and verified by several checks (see remark 1 and Section 4) reduces the required computational effort for the derivation of the zeros.

After obtaining the zeros, the change in their locations due to the changes in all the physical parameters of SRFB is thoroughly studied. It was shown that by increasing (or decreasing) the rigidity of the flexible section, EI, and the mass moment of inertia of the payload, I_{tip}, the zeros move further from (or become closer to) the imaginary axis; while by increasing (or decreasing) the mass per unit length of the flexible section, ρ, and the lengths of the rigid and flexible

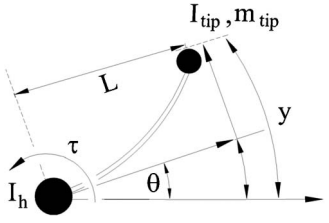

Fig. 1. Schematic of a slewing single flexible beam.

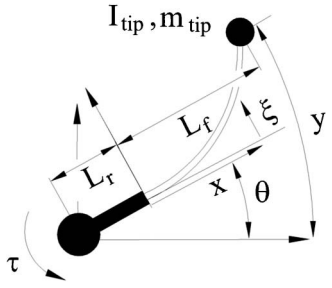

Fig. 2. The schematic of a SRFB.

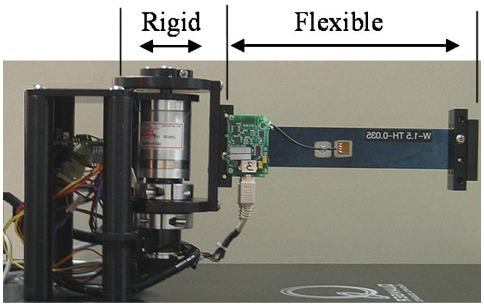

Fig. 3. SRFB installed in the Robotics Laboratory of the University of Saskatchewan.

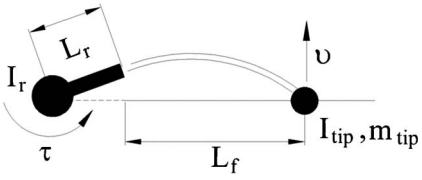

Fig. 4. The pinned-pinned counterpart of a SRFB which is shown in Fig. 2.

sections, L_r and L_f respectively, the zeros become closer to (or move further from) the imaginary axis. It is also observed that the change in the mass of the payload, m_{tip}, and mass moment of inertia of the rigid section, I_r, do not change the locations of the zeros.

The locations of the zeros and their changes due to the changes in the physical parameters were obtained in Sections 2 and 3 of this paper by using the infinite dimensional dynamic model of a SRFB, which did not include any truncation. However, truncated dynamic models of flexible link manipulators are widely used [1, 4, 6–8] for their ease of practical implementation [12]. The truncated dynamic models are also required for the numerical simulations of controllers, even when controllers are derived using infinite dimensional models [13]. Therefore, in Section 4 as a check, zeros of several different SRFBs which were modeled by a truncation method were compared with those that were found using the infinite dimensional dynamic model. After these comparisons, it was concluded that there were differences between the zeros of the truncated dynamic model and the infinite dimensional dynamic model. However, the same trend and behavior existed for the zeros of the infinite dimensional dynamic model and the zeros of the truncated dynamic models; see Section 4 for more details.

The novelties and contributions of this paper are: (*i*) a new theorem with its mathematical proof is introduced which simplifies the derivation of the zeros for a SRFB, (*ii*) a comprehensive study on the changes in the locations of the zeros due to the changes in all the physical parameters of a SRFB is reported, (*iii*) the physical parameters of a SRFB are classified into three different categories with respect to their effects on changing the locations of the zeros, and (*iv*) the physical parameters in these three different categories, which are found based on the infinite dimensional dynamic model, are shown to be as those that are obtained employing the truncated dynamic model. Thus, these new categorizations of the physical parameters can also be used when the truncated dynamic model is preferable.

2. ZEROS OF A SLEWING SINGLE RIGID-FLEXIBLE BEAM

In this paper the zeros of the SRFB will be calculated by adopting the theorem given in the previous section. That is, the SRFB is first pinned at the beam-end point as shown in Fig. 5, and then the zeros of transfer function, between the base torque and beam-end shear force, for this pinned-pinned beam are obtained.

The dynamic equation for the flexible portion of the SRFB in Fig. 5 is:

$$\rho\psi_{tt}(z,t)+EI\psi_{zzzz}(z,t)=0 \tag{1}$$

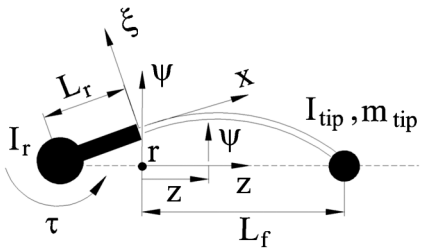

Fig. 5. Pinned-pinned counterpart of a SRFB which is shown in Fig. 2.

where z and ψ are measured from point r as shown in Fig. 5. Moreover, ρ is the mass per unit length of the flexible section, EI is the rigidity of the flexible section and $\psi_t(x,t)$ and $\psi_x(x,t)$ are the partial derivatives of $\psi(x,t)$ with respect to t and x, respectively, and a similar notation adopted for higher derivatives. The associated boundary conditions for this pinned-pinned beam are:

$$\psi(0,t) = L_r\,\psi_z(0,t) \tag{2a}$$

$$\psi(L_f,t) = 0 \tag{2b}$$

$$\tau + EI\psi_{zz}(0,t) - L_r EI\psi_{zzz}(0,t) = I_r\psi_{ztt}(0,t) \tag{2c}$$

$$EI\psi_{zz}(L_f,t) + I_{tip}\psi_{ztt}(L_f,t) = 0 \tag{2d}$$

where I_r is the mass moment of inertia of the rigid section with respect to the base, m_{tip} and I_{tip} are the mass and mass moment of inertia of the payload, L_f is the length of the flexible section and L_r is the length of the rigid section. Equation (2a) represents that the flexible section is clamped to the rigid section. Equation (2b), shows that the flexible section is pinned at the beam-end. Equations (2c) and (2d) represent the momentum balance for the rigid section and the payload, respectively. Taking the Laplace transform of Eq. (1) leads to:

$$\frac{d^4\psi(z,s)}{dz^4} - \lambda^4\psi(z,s) = 0 \tag{3}$$

where:

$$\lambda^4 = -\frac{\rho s^2}{EI} \tag{4}$$

and $\psi(z,s)$ is the Laplace transform of $\psi(z,t)$. From Eq. (3):

$$\psi(z,s) = c_1\cos(\lambda z) + c_2\sin(\lambda z) + c_3\cosh(\lambda z) + c_4\sinh(\lambda z) \tag{5}$$

and the unknown c_1, c_2, c_3 and c_4 are found by imposing the boundary conditions presented in Eqs. (2a–2d). Having $\psi(z,s)$ and also knowing that the shear force at the beam-end is $\upsilon(L_f,s) = EI\psi_{zzz}(L_f,s)$, the transfer function of the pinned-pinned beam counterpart of the SRFB is:

$$F(s)=\frac{EI\psi_{zzz}(L_f,s)}{\tau(s)}=\frac{N_F(s)}{D_F(s)} \tag{6}$$

where $N_F(s)$ and $D_F(s)$ are the numerator and denominator of the transfer function $F(s)$ and the output is the shear force. To find the zeros of $F(s)$ in Eq. (6), which are also the zeros of the transfer function $N(s) = y/\tau$ in Fig. 2, the condition $N_F(s) = 0$ has to be imposed, which results in:

$$\begin{aligned}&\left[\sin(\lambda L_f)+\sinh(\lambda L_f)+\lambda^3\left(\frac{I_{tip}}{\rho}\right)(\cos(\lambda L_f)-\cosh(\lambda L_f))\right]+\\ &L_r\left[\lambda(\cos(\lambda L_f)+\cosh(\lambda L_f))-\lambda^4\left(\frac{I_{tip}}{\rho}\right)(\sin(\lambda L_f)+\sinh(\lambda L_f))\right]=0\end{aligned} \tag{7}$$

By assuming $\beta = \lambda L_f$, Eqs. (4) and (7) are respectively :

$$s^2=-\beta^4\frac{EI}{\rho {L_f}^4} \tag{8}$$

$$\begin{aligned}&\left[\sin(\beta)+\sinh(\beta)+\beta^3\left(\frac{I_{tip}}{3I_{rb}}\right)(\cos(\beta)-\cosh(\beta))\right]+\\ &\frac{L_r}{L_f}\left[\beta(\cos(\beta)+\cosh(\beta))-\beta^4\left(\frac{I_{tip}}{3I_{rb}}\right)(\sin(\beta)+\sinh(\beta))\right]=0\end{aligned} \tag{9}$$

where $I_{rb}=\rho L_f^3/3$. Thus the zeros of a SRFB, that is the values of s, are obtained from Eq. (8) where β are the roots of Eq. (9). Since SRFB has infinite modes of vibration and for each mode of vibration there is a pair of zeros, the zeros of a SRFB are infinite. Thus, for a given L_r/L_f and I_{tip}/I_{rb}, Eq. (9) results in an infinite number of β values.

Remark 1: The zeros of a SRFB were also obtained by deriving the transfer function $G = y/\tau$ of Fig. 2 and were exactly the same as those obtained from Eqs. (8) and (9). This comparison was a check to verify the authors' new theorem.

3. ZEROS OBTAINED FROM EQUATIONS (8) AND (9)

The roots of Eq. (9) depend on the ratios I_{tip}/I_{rb} and L_r/L_f. To investigate the effect of these ratios on the locations of the zeros, Eq. (9) is solved numerically by writing a nonlinear solver in MATLAB. By using this solver, in Figs. (6a-7b) the zeros for the first two modes of vibration versus I_{tip}/I_{rb} and L_r/L_f are shown. From Eqs. (8) and (9) and Figs. (6a-7b) several observations were drawn which are:

1. The roots of Eq. (9) are independent on the rigidity of the flexible link, EI. The factor $EI/\rho L_f^4$ in Eq. (8) (n in Figs. (6a-7b)) represents the change in the locations of the zeros because of the change in the rigidity. Moreover, by increasing (or decreasing) the rigidity of the flexible section, while all other physical parameters are constant, the zeros move further from (or become closer to) the imaginary axis.

2. From view A in Figs. 6b and 7b, it is clear that the larger (or smaller) I_{tip}, the further from (or the closer to) the imaginary axis the zeros are, assuming all other physical parameters are constant.

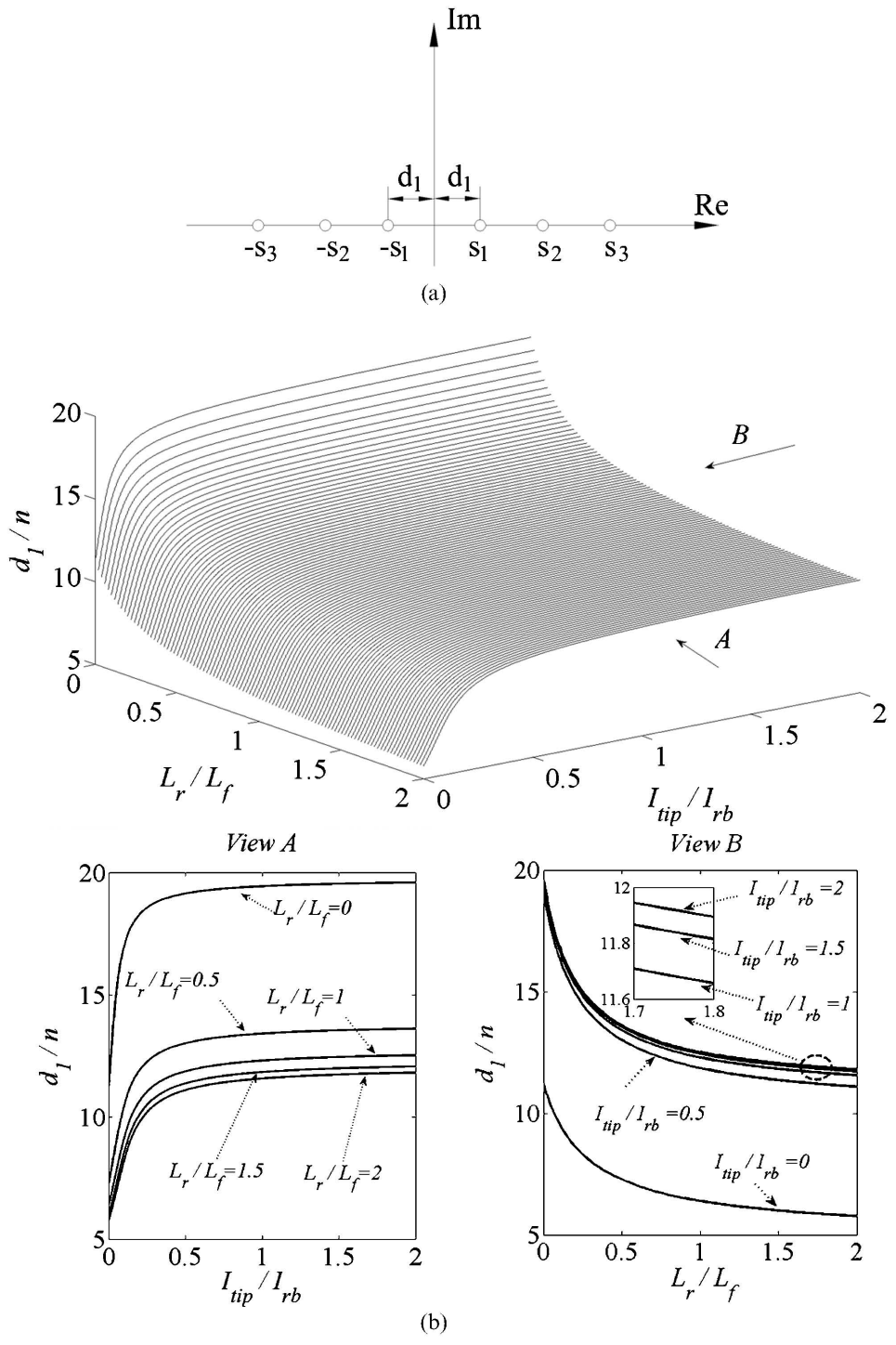

Fig. 6. (a) Schematic of the zeros of the first vibration mode, $(-s_1,s_1)$; (b) Variation of d_1 in Fig. 6a versus I_{tip}/I_{rb} and L_r/L_f ($n=\sqrt{EI/\rho L_f^4}$,$I_{rb}=\rho L_f^3/3$).

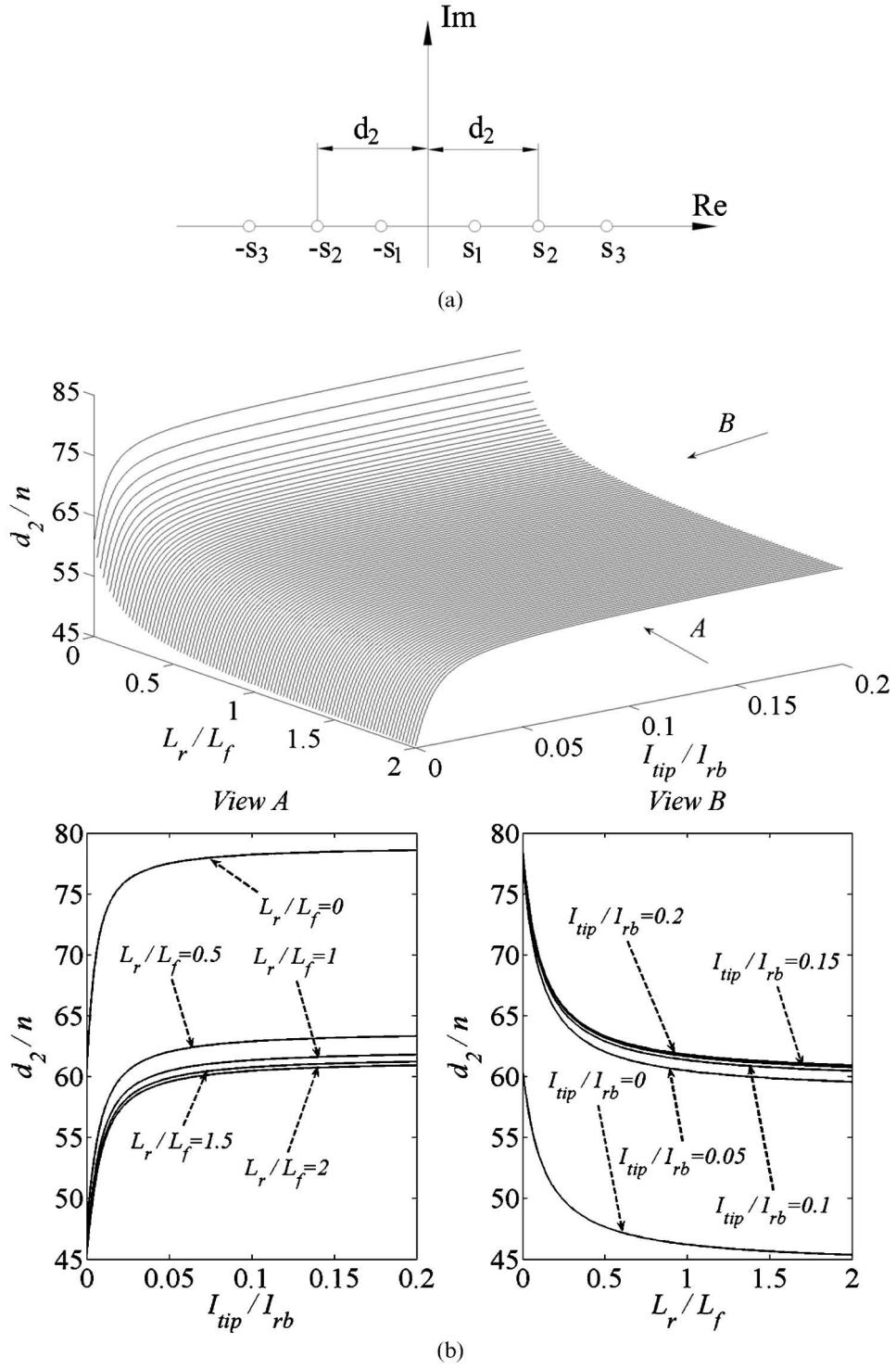

Fig. 7. (a) Schematic of the zeros of the second vibration mode, $(-s_2,s_2)$; (b) Variation of d_2 in Fig. 7a versus I_{tip}/I_{rb} and L_r/L_f ($n=\sqrt{EI/\rho L_f^4}, I_{rb}=\rho L_f^3/3$).

3. While the locations of the zeros depend on the value of I_{tip}, these locations are independent of the value of m_{tip}. That is, the locations of the zeros do not change by changing m_{tip}, as long as I_{tip} is constant. This can be concluded since m_{tip} did not appear in Eqs. (8) and (9) which determine the locations of the zeros. This independence of the zeros to the mass of the payload m_{tip} agrees with the physical interpretation of the zeros given in [14] and has also been mentioned in [12] for a flexible beam shown in Fig. 1.
4. The locations of the zeros of a SRFB are independent of the mass moment of inertia of the rigid portion I_r. This can be concluded since I_r did not appear in Eqs. (8) and (9) which determine the locations of the zeros.
5. From View B in Figs. 6b and 7b, it is clear that the larger (or smaller) L_r, the closer to (the further from) the imaginary axis the zeros are, assuming all other physical parameters are constant.
6. The larger (or smaller) L_f, the closer to (the further from) the imaginary axis the zeros are, assuming all other physical parameters are constant. This conclusion cannot be drawn from Figs. 6b and 7b since by changing L_f, the ratios L_r/L_f, $n=\sqrt{EI/\rho L_f^4}$ and I_{tip}/I_{rb} will change. However, the variation of the zeros of the first two mode shapes of a SRFB, shown in Figs. 8a and 8b versus L_f/L_r, clearly indicates the further movement of zeros from imaginary axis by decreasing L_f. In Figs. 8a and 8b, contrary to Figs. 7a and 7b, by changing L_f only the ratio L_f/L_r will be changed. To draw Figs. 8a and 8b, Eqs. (8) and (9) were rearranged and solved as detailed in Appendix I of [15].
7. The larger (or smaller) the mass per unit length of the beam ρ, the closer to (or the further from) the imaginary axis the zeros are. This conclusion can easily be drawn from Figs. 9a and 9b where these figures were obtained from Figs. 6b and 7b with the details provided in Appendix II of [15].

Thus, the physical parameters of the SRFB can be divided into three categories with regard to changing the locations of the zeros. These categories are defined in Table 1.

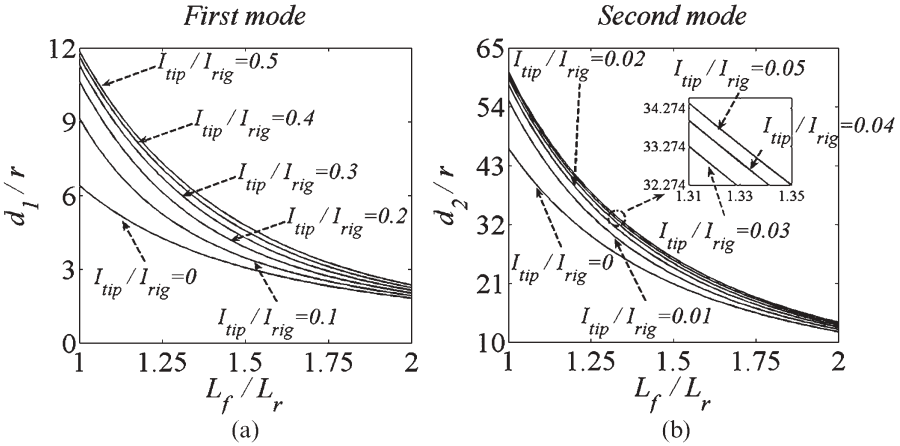

Fig. 8. (a). Variation of d_1 in Fig. 6a versus L_f/L_r; (b) Variation of d_2 in Fig. 7a. versus L_f/L_r ($r=\sqrt{EI/\rho L_r^4}, I_{rig}=\rho L_r^3/3$).

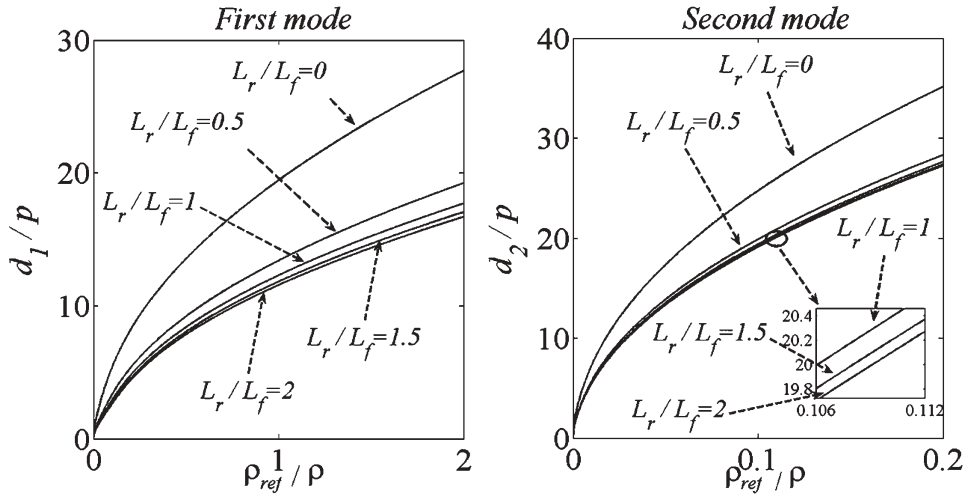

Fig. 9. (a) Variation of d_1 in Fig. 6a versus ρ; (b) Variation of d_2 in Fig. 7a versus ρ ($p=\sqrt{EI/3I_{tip}L_f}, \rho_{ref}=3I_{tip}/L_f^3$).

4. ZEROS OBTAINED BY USING THE ASSUMED MODE SHAPE METHOD

The approach taken in Section 2 and the results presented in Section 3, which are summarized in Table 1, are based on the infinite dimensional dynamic model of a SRFB which does not have any truncation. However, truncated dynamic model of flexible manipulators are widely used [1, 4, 6–8, 18, 19]. This is for the ease of the practical implementation of the truncation dynamic models. Moreover, truncated dynamic models are used for the simulation study of controllers, even when controllers are designed using the infinite dimensional model [13]. Nevertheless, the truncated dynamic models may lead to the so-called spillover instability in the experimental implementation of the controllers [20–22]. This instability is due to the contribution of vibration modes that are not considered in the truncated model. Since controller design is based on the considered modes of vibration, excitation of un-modeled modes, may lead to closed-loop instability.

In this section the extension of the findings in Table 1 to the cases where truncated dynamic models were preferred was explored. The assumed mode shape method (AMM) [16] was used

Table 1. The three categories for the physical parameters of a SRFB.

Category number	Physical parameters in the category	By increasing (decreasing) the physical parameter in the category, the zeros
One	$I_{tip}(kg.m^2)$, $EI(N.m^2)$	move further from (become closer to) the imaginary axis
Two	$\rho(kg/m)$, $L_r(m)$, $L_f(m)$	become closer to (move further from) the imaginary axis
Three	$m_{tip}(kg)$, $I_r(kg.m^2)$	do not move

here to derive the truncated dynamic model of a SRFB. Based on this method the lateral deflection of the beam, ξ in Fig. 2, was modeled as:

$$\xi(x,t) = \sum_{i=1}^{w} \gamma_i(t)\phi_i(x) \tag{10}$$

where $\phi_i(x)$ is the ith assumed mode shapes, $\gamma_i(t)$ is its time varying weight function and w is the number of mode shapes used to model the flexibility. By using Eq. (10), the generalized coordinate of a SRFB is finite and the vector composed of these coordinates is:

$$q = [\,\theta \quad \gamma_1 \quad \dots \quad \gamma_w\,]^T \tag{11}$$

where θ is shown in Fig. 2 and $\gamma_i(t)$ is defined in Eq. (10). Each of these generalized coordinates, based on the Hamiltonian principle, must satisfy following Lagrange equation:

$$\frac{d}{dt}\left(\frac{\partial T_{SRFB}}{\partial \dot{q}_i}\right) - \frac{\partial T_{SRFB}}{\partial q_i} + \frac{\partial U_{SRFB}}{\partial q_i} = Q_i \qquad (i = 1 \dots w+1) \tag{12}$$

where, T_{SRFB} is the kinetic energy of the SRFB, U_{SRFB} is the strain energy of SRFB due to the beam's flexibility, q_i is the ith element of the vector q in Eq. (11), and Q_i is the generalized force corresponding to q_i; See [16] for more details. By employing the Lagrange equation, Eq. (12), the dynamic equation of a SRFB is:

$$M\,\ddot{q} + K\,q = H\,\tau \tag{13}$$

where M is the mass matrix, K is the stiffness matrix, q is defined in Eq. (11), and H is a constant matrix which maps the input torque τ to its corresponding generalized coordinates. Details of all these matrices are available in [16].

Equation (13) is a linear dynamic model. This equation is obtained by assuming that the lateral deflection of the flexible beam is small. Based on this assumption, (*i*)- nonlinear terms for a beam in bending [23] can be neglected in the expression of the potential energy U_{SRFB} and, (*ii*)- quadratic terms containing γ_i^2, where γ_i is defined after Eq. (10), can be neglected [24] in the kinetic energy expression T_{SRFB}. By neglecting these nonlinear effects, the dynamic model of a SRFB will be linear [16]. To consider all these nonlinearities when the link's lateral deflection is large, finite element analysis can be used as presented by authors in [25, 26]. It should be noted that to derive the zeros of a SRFB, a linear dynamic model of SRFB is required since the transfer function and consequently the zeros are defined for linear systems.

The state-space representation for Eq. (13), assuming the end-beam displacement is the output will be:

$$\begin{cases} \dot{X} = A_{SRFB}\,X + B_{SRFB}\,\tau \\ \qquad y = C_{SRFB}\,X \end{cases} \tag{14}$$

where

$$A_{SRFB}=\begin{bmatrix} 0_{w+1\times w+1} & I_{w+1\times w+1} \\ -M^{-1}K & 0_{w+1\times w+1} \end{bmatrix} \quad B_{SRFB}=\begin{bmatrix} 0 \\ M^{-1}H \end{bmatrix} \tag{15}$$
$$X^T=\begin{bmatrix} q^T & \dot{q}^T \end{bmatrix} \qquad C_{SRFB}=\lfloor (L_r+L_f) \quad \phi_1(L_f) \quad \ldots \quad \phi_w(L_f) \quad 0_{1\times(w+1)} \rfloor$$

In Eq. (14), A_{SRFB} is the state matrix, B_{SRFB} is the input matrix, and C_{SRFB} is the output matrix. Also $I_{w+1\times w+1}$ and $0_{w+1\times w+1}$ are respectively an identity and zero matrices of order $w+1\times w+1$. From the state-space representation of a SRFB, the transfer function y/τ is [17]:

$$\frac{y}{\tau}=C_{SRFB}(sI_{2(w+1)\times 2(w+1)}-A_{SRFB})^{-1}B_{SRFB} \tag{16}$$

and then the zeros of a SRFB which is modeled by the AMM, are the zeros of the above transfer function.

For simplicity and without loss of generality, the zeros corresponded to the first mode of vibration were found and compared with each other in the following. The acronym "AMM zeros" used for the zeros obtained based on the AMM, zeros of Eq. (16), while "IDM zeros" referred to the zeros obtained based on the infinite dimensional dynamic model, Eqs. (8) and (9).

4.1. Category number one in Table 1 (I_{tip}, EI)

In Fig. 10 the IDM and AMM zeros for different SRFB are shown, where only the mass moment of the inertias of the payloads, I_{tip}, are different. The rest of physical parameters are the same and given in the caption of this figure. The values for some of the AMM zeros and IDM zeros versus I_{tip} are also provided in Table 2. The parameter $DBIA$ in Table 2 is defined as:

$$DBIA=IDM\ zero-AMM\ zero \tag{17}$$

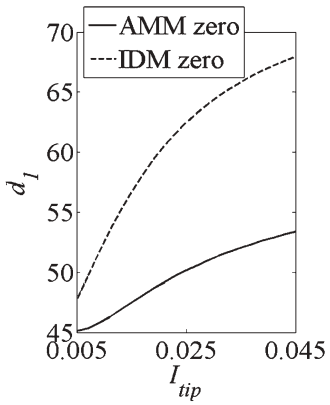

Fig. 10. Schematic of AMM and IDM zeros v.s. I_{tip}, (EI = 16, ρ = *0.8*, m_{tip} = 2, I_r = 0.003, L_r = 0.1, L_f = 1.0), units are in SI.

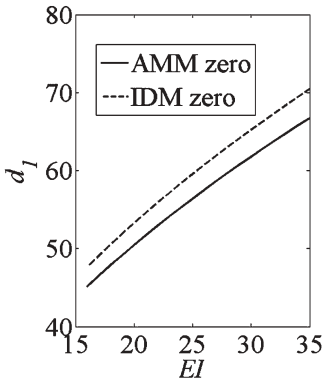

Fig. 11. Schematic of AMM and IDM zeros v.s. EI, (ρ = *0.8*, m_{tip} = 2, I_r = 0.003, L_r = 0.1, L_f = 1.0, I_{tip} = 0.005), units are in SI.

Table 2. AMM and IDM zeros as well as their differences for different I_{tip}, (the rest of the physical parameters were as in Fig. 10)

$I_{tip}(kg.m^2)$	AMM	IDM	***DBIA***
0.005	45.12	47.64	2.520
0.007	45.33	49.62	4.290
0.009	45.75	51.56	5.810
0.011	46.28	53.40	7.120
0.013	46.88	55.11	8.230
0.015	47.48	56.68	9.200
0.017	48.07	58.10	10.03
0.019	48.64	59.37	10.73
0.021	49.17	60.52	11.35
0.023	49.68	61.54	11.86
0.025	50.15	62.45	12.30
0.027	50.58	63.27	12.69
0.029	50.99	64.01	13.02
0.031	51.37	64.68	13.31
0.033	51.72	65.28	13.56
0.035	52.04	65.82	13.78
0.037	52.34	66.32	13.98
0.039	52.63	66.77	14.14
0.041	52.89	67.19	14.30
0.043	53.14	67.57	14.43

In Fig. 11 the IDM and AMM zeros for different SRFB are given, where only the rigidities of the flexible sections, *EI*, are different. The rest of physical parameters are constant and provided in the caption of Fig. 11. The values for some of the AMM zeros and IDM zeros versus *EI* are also given in Table 3.

Form Figs. 10, 11, Tables 2 and 3, it is clear that by increasing (or decreasing) I_{tip} and *EI*, the AMM zeros move further from (or become closer to) the imaginary axis, similar to IDM zeros. That is d_1 in Figs. 10 and 11, or the values of AMM zeros in Tables 2 and 3, increase (or decrease) by increasing (or decreasing) I_{tip} and *EI*. This confirm that I_{tip} and *EI* are indeed in the category number one in Table 1. Moreover, from Tables 2 and 3 it can be observed that by increasing I_{tip} and *EI*, the difference between AMM zeros and IDM zeros increases; that is the value of *DBIA* increases. By increasing I_{tip} from 0.005 ($kg.m^2$) to 0.043 ($kg.m^2$), *DBIA* increases from 2.52 to 14.43. The increase in *DBIA* is from 2.52 to 3.72 when *EI* increases from 16 ($N.m^2$) to 35($N.m^2$).

4.2. Category number two in Table 1 (ρ, L_r, L_f)

In Figs. 12–14 the AMM and IDM zeros of different SRFB are shown. In Fig. 12 only the densities per unit lengths of the flexible sections, ρ, are different, in Fig. 13 the lengths of the rigid sections, L_r, are changed and in Fig. 14 only the lengths of the flexible sections, L_f, are varied. The rest of the physical parameters for each figure are constant and given in the captions of these figures. The sample numerical values which correspond to Figs. 12–14 are given in Tables 4–6, respectively. From these figures and tables it can be seen that by increasing (or decreasing) ρ, L_r and L_f, AMM zeros become closer to (or move further from) the imaginary

Table 3. AMM and IDM zeros as well as their differences for different *EI* (The rest of the physical parameter were as in Fig. 11).

$EI(N.m^2)$	AMM	IDM	***DBIA***
16	45.12	47.64	2.520
17	46.51	49.10	2.590
18	47.86	50.53	2.670
19	49.17	51.91	2.740
20	50.45	53.26	2.810
21	51.69	54.58	2.890
22	52.91	55.86	2.950
23	54.10	57.12	3.020
24	55.26	58.34	3.080
25	56.40	59.55	3.150
26	57.52	60.73	3.210
27	58.62	61.88	3.260
28	59.69	63.02	3.330
29	60.75	64.14	3.390
30	61.79	65.23	3.440
31	62.81	66.31	3.500
32	63.81	67.37	3.560
33	64.80	68.42	3.620
34	65.78	69.44	3.660
35	66.74	70.46	3.720

axis; that is d_1 in Figs. 12–14 decreases (or increases) by increasing (or decreasing) ρ, L_r and L_f. Thus these parameters fall into category number two in Table 1. Moreover by increasing the densities per unit lengths of the flexible sections, ρ, and the lengths of the rigid sections, L_r, the difference between AMM and IDM zeros becomes smaller; that is *DBIA* reduces. By increasing ρ from 0.50 (*kg*/*m*) to 1.45 (*kg*/*m*), *DBIA* reduces from 6.41 to 0.320. The reduction in *DBIA* is from 2.52 to 1.12 when L_r increases from 0.10 (*m*) to 0.29 (*m*). Finally, as L_f increases from 1.00

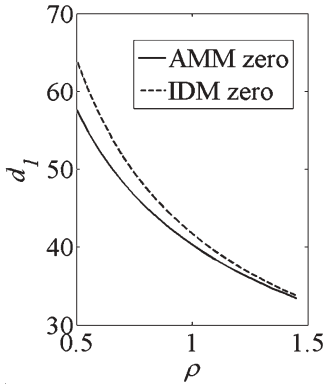

Fig. 12. Schematic of AMM and IDM zeros v.s. ρ, ($EI = 16, L_r = 0.1, m_{tip} = 2, I_r = 0.003, I_{tip} = 0.005, L_f = 1.0$), units are in SI.

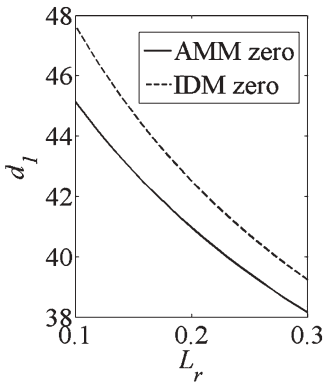

Fig. 13. Schematic of AMM and IDM zeros v.s. L_r, ($\rho = 0.8, m_{tip} = 2, I_r = 0.003, EI = 16, L_f = 1.0, I_{tip} = 0.005$), units are in SI.

Table 4. AMM and IDM zeros as well as their differences for different ρ, (the rest of the physical parameters were as in Fig. 12).

$\rho(kg/m)$	AMM	IDM	***DBIA***
0.50	57.59	64.00	6.410
0.55	54.76	64.17	5.410
0.60	52.33	56.92	4.590
0.65	50.20	54.12	3.920
0.70	48.31	51.69	3.380
0.75	46.63	49.54	2.910
0.80	45.12	47.64	2.520
0.85	43.75	45.93	2.180
0.90	42.50	44.39	1.890
0.95	41.35	42.99	1.640
1.00	40.29	41.72	1.430
1.05	39.31	40.55	1.230
1.10	38.40	39.47	1.070
1.15	37.55	38.47	0.920
1.20	36.76	37.54	0.780
1.25	36.00	36.68	0.680
1.30	35.30	35.87	0.570
1.35	34.63	35.11	0.480
1.40	34.01	34.22	0.390
1.45	33.41	33.73	0.320

(m) to 1.30 (m), *DBIA* reduces from 2.52 to 0.03, by increasing L_f from 1.30(m) to 1.8 (m), (absolute value of) *DBIA* increases from 0.03 to 0.39, and when L_f increases from 1.8 (m) to 2.0 (m), (absolute value of) *DBIA* reduces from 0.39 to 0.36.

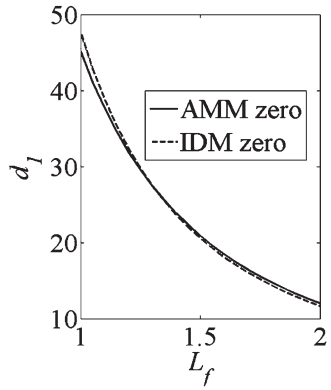

Fig. 14. Schematic of AMM and IDM zeros v.s. L_f ($EI = 16$, $I_{tip} = 0.005$, $m_{tip} = 2$, $I_r = 0.003$, $\rho = 0.8$, $L_f = 1.0$)' units are in SI.

Table 5. AMM and IDM zeros as well as their differences for different L_r (The rest of the physical parameter were as in Fig. 13).

$L_r(m)$	AMM	IDM	*DBIA*
0.10	45.12	47.64	2.520
0.11	44.62	47.01	2.390
0.12	44.13	46.38	2.250
0.13	43.67	45.82	2.150
0.14	43.23	45.26	2.030
0.15	42.81	44.76	1.950
0.16	42.41	44.25	1.840
0.17	42.03	43.79	1.760
0.18	41.66	43.34	1.680
0.19	41.30	42.92	1.620
0.20	40.96	42.50	1.540
0.21	40.63	42.12	1.490
0.22	40.32	41.74	1.420
0.23	40.01	41.39	1.380
0.24	39.72	41.04	1.320
0.25	39.44	40.71	1.270
0.26	39.16	40.39	1.230
0.27	38.90	40.09	1.190
0.28	38.64	39.79	1.150
0.29	38.40	39.52	1.120

4.3. Category number three in Table 1 (m_{tip},I_r)

In Figs. 15 and 16, IDM and AMM zeros of different SRFB are presented, where only the masses of the payloads, m_{tip}, or the mass moment of inertias of the rigid sections, I_r, are different. The values for the rest of the physical parameters are unchanged and provided in the captions. The numerical values for some of the points on Figs. 15 and 16 are given in Tables 7 and 8, respectively. From these figures and the values given in Tables 7 and 8, it is obvious that

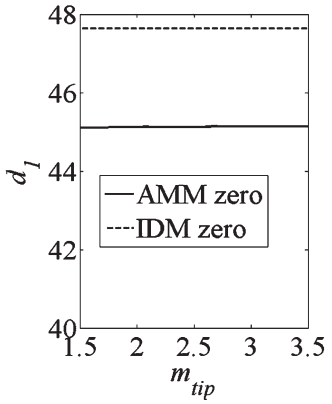

Fig. 15. Schematic of AMM and IDM zeros v.s. m_{tip}, ($EI = 16$, $L_r = 0.1$, $\rho = 0.8$, $I_r = 0.003$, $I_{tip} = 0.005$, $L_f = 1.0$), units are in SI.

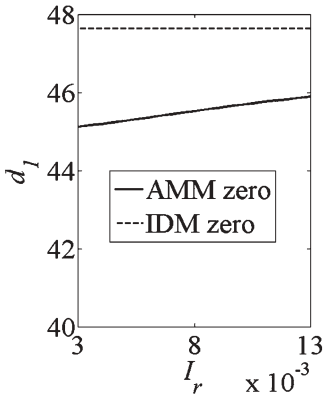

Fig. 16. Schematic of AMM and IDM zeros v.s. I_r, ($\rho = 0.8$, $m_{tip} = 2$, $L_r = 0.1$, $EI = 16$, $L_f = 1.0$, $I_{tip} = 0.005$), units are in SI.

Table 6. AMM and IDM zeros as well as their differences for different L_f,(the rest of the physical parameter were as in Fig. 14).

$L_f(m)$	AMM	IDM	***DBIA***
1.00	45.12	47.64	2.52
1.05	41.12	42.89	1.77
1.10	37.64	38.85	1.21
1.15	34.61	35.38	0.77
1.20	31.93	32.37	0.44
1.25	29.55	29.75	0.20
1.30	27.43	27.46	0.03
1.35	25.53	25.43	-0.10
1.40	23.82	23.63	-0.19
1.45	22.28	22.01	-0.27
1.50	20.88	20.56	-0.32
1.55	19.61	19.26	-0.35
1.60	18.45	18.07	-0.38
1.65	17.39	17.00	-0.39
1.70	16.41	16.02	-0.39
1.75	15.52	15.13	-0.39
1.80	14.70	14.31	-0.39
1.85	13.94	13.56	-0.38
1.90	13.24	12.86	-0.38
1.95	12.59	12.22	-0.37
2.00	11.99	11.63	-0.36

no significant changes in the AMM zeros occur by changing m_{tip} and I_r. From Table 7, the maximum difference between all the AMM zeros for different m_{tip} is only 0.03, which is the difference between 45.11 (for $m_{tip} = 1.5(kg)$) and 45.14 (for $m_{tip} = 3.4(kg)$). From Table 8, the maximum difference between all AMM zeros for different I_r is only 0.74. This difference is from 45.12 (for $I_r = 0.0030(kg.m^2)$) to 45.86 (for $I_r = 0.0125(kg.m^2)$). Moreover, from Tables 7 and 8, it is clear the IDM zeros do not changes for different m_{tip} and I_r as stated in Section 3. Therefore, m_{tip} and I_r are members of the category number three in Table 1, regardless of using the assumed mode shape model or infinite dimensional dynamic model. It is worth noting that small variations in the AMM zeros when m_{tip} and I_r are changed can be due to the truncation [18, 19] and are acceptable.

Remark 2: From the results presented in Section 4-1 to 4-3, it is concluded that the findings in Table 1 are also valid when AMM are employed to model the beam flexibility. From these results, it can be seen that the differences between the zeros of these two different modeling methods, *DBIA*, varied between 0.03 and 14.55, as the physical parameters changed. Future research will address the condition when this difference is small.

5. CONCLUSIONS

A slewing single rigid-flexible beam (SRFB), which had a rigid beginning section was considered. A comprehensive study on the zeros of its transfer function, between the beam-end displacement and the base torque, was performed. The infinite dimensional dynamic model of

Table 7. AMM and IDM zeros as well as their differences for different m_{tip}, (the rest of the physical parameters were as in Fig. 15).

$m_{tip}(kg)$	AMM	IDM	***DBIA***
1.50	45.11	47.64	2.530
1.60	45.11	47.64	2.530
1.70	45.11	47.64	2.530
1.80	45.12	47.64	2.520
1.90	45.12	47.64	2.520
2.00	45.12	47.64	2.520
2.10	45.13	47.64	2.510
2.20	45.13	47.64	2.510
2.30	45.13	47.64	2.510
2.40	45.13	47.64	2.510
2.50	45.13	47.64	2.510
2.60	45.13	47.64	2.510
2.70	45.14	47.64	2.500
2.80	45.14	47.64	2.500
2.90	45.14	47.64	2.500
3.00	45.14	47.64	2.500
3.10	45.14	47.64	2.500
3.20	45.14	47.64	2.500
3.30	45.14	47.64	2.500
3.40	45.14	47.64	2.500

Table 8. AMM and IDM zeros as well as their differences for different I_r (The rest of the physical parameter were as in Fig. 16).

$I_r(kg.m^2)$	AMM	IDM	***DBIA***
0.0030	45.12	47.64	2.520
0.0035	45.16	47.64	2.480
0.0040	45.19	47.64	2.450
0.0045	45.23	47.64	2.410
0.0050	45.27	47.64	2.370
0.0055	45.31	47.64	2.330
0.0060	45.35	47.64	2.290
0.0065	45.40	47.64	2.240
0.0070	45.44	47.64	2.200
0.0075	45.48	47.64	2.160
0.0080	45.52	47.64	2.120
0.0085	45.56	47.64	2.080
0.0090	45.60	47.64	2.040
0.0095	45.64	47.64	2.000
0.0100	45.68	47.64	1.960
0.0105	45.72	47.64	1.920
0.0110	45.76	47.64	1.880
0.0115	45.79	47.64	1.850
0.0120	45.83	47.64	1.820
0.0125	45.86	47.64	1.780

SRFB was used for this study with no truncation. Thus the locations of the zeros were found accurately. It was shown, for the first time, that the physical parameters of a SRFB fall into three categories with regard to changing the locations of the zeros. The first category was composed of the mass moment of inertia of the payload and the rigidity of the flexible portion, whereby increasing (or decreasing) these parameters caused the zeros to move further from (or to become closer to) the imaginary axis. The second category was composed of the mass per unit length of the flexible section and the lengths of the rigid and flexible sections, whereby increasing (or decreasing) these physical parameters caused the zeros to become closer to or (move further from) the imaginary axis. The third category was composed of the mass moment of inertia of the rigid section and the mass of the payload. In this category no change in the location of the zero will occur by changing these physical parameters.

Several SRFB with different physical parameters were considered and their zeros were obtained by modeling them according to the assumed mode shape truncation method. The changes in the locations of these zeros due to the changes in all the physical parameters were studied. It was concluded that the changes in zeros have similar trends as those of the zeros derived by using the infinite dimensional dynamic model. This proved that the categorization of the physical parameters, introduced in this paper, can also be used where the truncated dynamic model is preferable. However the zeros of a truncated dynamic model and an infinite dimensional model were different. These differences varied, from 0.36 to 14.55, for different physical parameters. The smaller this difference the better the truncation is. A future study will address the conditions where this difference is small.

REFERENCES

1. Wang, F. Y. and Gao, Y., *Advanced studies of flexible robotic manipulators: modeling, design, control and applications*, World Scientific, New Jersey, USA, 2003.
2. Slotine, J. J. and Li, W., *Applied nonlinear control*, Prentice Hall, NJ, USA, 1991.
3. Hoagg, J.B. and Bernstein, D.S., ''Nonminimum-phase zeros,'' *IEEE Control Systems Magazine*, Vol. 45, pp. 45–57, 2007.
4. Paden, B., Chen, D., Ledesma, R. and Bayo, E., ''Exponentially stable tracking tontrol for multi-joint flexible-link manipulators,'' *ASME Journal of Dynamic Systems, Measurement and Control*, Vol. 115, pp. 53–59, 1993.
5. Devasia, S., ''Approximated stable inversion for nonlinear system with nonhyperbolic internal dynamics,'' *IEEE Transactions on Automatic Control*, Vol. 44, No. 7, pp. 1419–1425, 1999.
6. Wang, X. and Chen, D., ''Output tracking control of a one-link flexible manipulator via causal inversion,'' *IEEE Transactions on Control System Technology*, Vol. 14, No. 1, pp. 141–148, 2006.
7. Feng, Y., Bao, B. and Yu, X., ''Inverse dynamics nonsingular terminal sliding mode control of two-link flexible manipulator,'' *International Journal of Robotics and Automations*, Vol. 19, No. 2, pp. 91–102, 2004.
8. Moallem, M., Patel, R.V. and Khorasani, K., *Flexible-link robot manipulators, Control techniques and Structural design*, Springer, London, 2000.
9. Park, H.S., Chang, P. H. and Lee, D.Y., ''Trajectory planning for the tracking control of systems with unstable zeros,'' *Mechatronics*, Vol. 13, pp. 127–139, 2003.
10. Vakil, M., Fotouhi, R. and Nikiforuk, P.N., ''Zeros of the transfer function of a rigid-flexible manipulator,'' *the 21st Canadian Congress of Applied Mechanics*, Toronto, Ontario, Canada, Paper No. GP_75 (CD Rom), 2007.

11. Vakil, M., Fotouhi, R. and Nikiforuk, P.N., ''On the zeros of the transfer function of a single flexible link manipulator,'' *17th IASTED International conference on Modeling and Simulation*, Montreal, Quebec, Canada, pp.20–25, 2006.
12. Spector, V.A. and Flashner, H., ''Modeling and design implications of noncollocated control in flexible systems,'' *Journal of Dynamic Systems, Measurement and Control*, Vol. 112, No. 2, pp. 186–193, 1990.
13. Jalili, N., ''An infinite dimensional distributed based controller for regulation of flexible robot arms,'' *Journal of Dynamic Systems, Measurement and Control*, Vol. 123, No. 4, pp. 712–719, 2001.
14. Miu, D.K., ''Physical interpretation of transfer function zeros for simple control systems with mechanical flexibility,'' *Journal of Dynamic Systems, Measurement and Control*, Vol. 13, No. 3, pp. 419–424, 1991.
15. Vakil, M., Fotouhi, R. and Nikiforuk, P.N., ''Further results on the zeros of a slewing single rigid-flexible manipulator,'' *Canadian Committee for the Theory of Machines and Mechanisms Symposium*, Québec, Canada, Paper No. CCToMM09-P24 (CD Rom), 2009.
16. Vakil, M., Fotouhi, R. and Nikiforuk, P.N., ''Causal end-effector inversion of a flexible link manipulator,'' *Mechatronics*, in press, 2009.
17. Ogata, K., *Modern control engineering*, Prentice Hall, NJ, USA, 1996.
18. Fraser, A.R. and Daniel, R.W., *Perturbation techniques for flexible manipulators, Kulwer Academic Publishers*, Boston, USA, 1991.
19. Moheimani, S.O.R. and Clark, R.L., ''Minimizing the truncation error in assumed mode models for structures,'' *Journal of Vibration and Acoustics*, Vol. 122, No. 3, pp. 332–3325, 2000.
20. Ohta, H., Nikiforuk, P.N. and Aoki, T., ''Spillover prevention and control of flexible structures using modal filters,'' *Control, Theory and Advanced Technology*, Vol. 4, No. 1, pp. 15–35, 1988.
21. Balas, M. J., ''Modal control of certain flexible dynamic systems,'' *SIAM Journal on Control and Optimization*, Vol. 16, No. 3, pp. 450–462, 1987.
22. Caracciolo, R., Richiedei, D., Trevisani, A. and Zanotto, A., ''Robust mixed-norm position and vibration control of flexible link mechanisms,'' *Mechatronics*, Vol. 15, No. 7, pp. 767–791, 2005.
23. Prezemienechi, J. S., *Theory of matrix structural analysis*, McGraw Hill, NY, USA, 1967.
24. Vakil, M., Fotouhi, R. and Nikiforuk, P. N., ''Trajectory tracking for the end-effector of a class of flexible link manipulators,'' *Journal of Vibration and Control*, in press, 2009, DOI: 10.1177/1077546309350554
25. Fotouhi, R., ''Dynamic analysis of very flexible beams,'' *Journal of Sound and Vibration*, Vol. 305, pp. 521–533, 2007.
26. Vakil, M., Fotouhi, R. and Nikiforuk, P. N., ''A Constrained Lagrange formulation of multilink planar flexible manipulator,'' *ASME Journal of Vibration and Acoustics*, Vol. 130, No. 3, pp. 1–16, 2008.

APPENDIX I: PROOF OF THE NEW THEOREM USED FOR THE DERIVATION OF THE ZEROS.

In the following, a lemma with its proof will be first given and it will then be used in the proof of new theorem which is introduced in this paper for the derivation of the zeros.

Lemma: *Consider the transfer function G(s):*

$$G(s) = Y(s)/\tau(s) = N_G(s)/D_G(s) = \sum_{i=0}^{n} a_i s^i / \sum_{i=0}^{m} b_i s^i \tag{A1}$$

where $Y(s)$ and $\tau(s)$ are the Laplace transformations of the output $y(t)$ and input $\tau(t)$ respectively, $N_G(s)$ and $D_G(s)$ represent the numerator and denominator of the transfer function $G(s)$ respectively, n and m are the orders of the numerator and denominator polynomials respectively, and s is the Laplace parameter. Also, assume that the output $y(t)$satisfies the following initial conditions:

$$y^{(i)}(0)=0, i=1,\ldots,m-1 \tag{A2}$$

where $y^{(i)}$ is the i^{th} time derivative of y. Then for this transfer function the input $\tau(t) = e^{wt}$ makes the output $y(t)$ goes to zero, if and only if w is a zero of the transfer function $G(s)$ or equally a root of the numerator $N_G(s) = 0$.

Proof of the lemma: From Eq. (A1) the differential equation between the outputs $y(t)$ to the input $\tau(t)$ is:

$$(\sum_{i=0}^{m} b_i \frac{d^i}{dt^i})y(t)=(\sum_{i=0}^{n} a_i \frac{d^i}{dt^i})\tau(t) \tag{A3}$$

Sufficiency: For $\tau(t) = e^{wt}$ where w is a root of $N(s) = 0$, the RHS of Eq. (A3) is zero. Thus:

$$(\sum_{i=0}^{m} b_i \frac{d^i}{dt^i})y(t)=0 \tag{A4}$$

Considering Eq. (A4) and the initial conditions provided in Eq. (A2), then $y(t)$ and all its time derivatives are zero.

Necessity: Replacing $\tau(t) = e^{wt}$ in Eq. (A3) leads to:

$$(\sum_{i=0}^{m} b_i \frac{d^i}{dt^i})y(t)=(a_0+a_1w+a_2w^2\cdots)e^{wt}=(\sum_{i=0}^{n} a_i w^i)\, e^{wt} \tag{A5}$$

If for $\tau(t) = e^{wt}$ the output $y(t)$ is zero, then Eq. (A5) results in:

$$(a_0+a_1w+a_2w^2\cdots)e^{wt}=0 \tag{A6}$$

Or

$$(a_0+a_1w+a_2w^2\cdots)=0 \tag{A7}$$

and thus w is indeed a root of $N_G(s) = 0$.

Proof of the new theorem used for the derivation of the zeros which is presented on page 2: The governing dynamic equations for a SRFB, shown in Fig. 2, are:

$$\rho((x+L_r)\ddot{\theta}+\xi_{tt}(x,t))+EI\xi_{xxxx}(x,t)=0 \tag{A8}$$

$$I_r\ddot{\theta} = \tau + EI\xi_{xx}(0,t) + L_r EI\xi_{xxx}(0,t) \tag{A9}$$

with the boundary conditions:

$$\xi(0,t) = 0 \tag{A10}$$

$$\xi_x(0,t) = 0 \tag{A11}$$

$$EI\xi_{xxx}(L_f,t) = m_{tip}((L_r + L_f)\ddot{\theta} + \xi_{tt}(L_f,t)) \tag{A12}$$

$$EI\xi_{xx}(L_f,t) = -I_{tip}(\ddot{\theta} + \xi_{xtt}(L_f,t)) \tag{A13}$$

where x is measured from the end of the rigid section, ξ is the lateral deflection of the slewing flexible section, and the rest of the parameters are as those defined after Eqs. (1) and/or Eqs. (2a–2d). Equations (A8) and (A9) are the force balance for an element of the flexible part and momentum balance for the rigid section of the link, respectively, Eqs. (A10) and (A11) are due to the fact that the flexible link is clamped to the rigid part, and Eqs. (A12) and (A13) represent the force and momentum balance for the payload, respectively.

From the above Lemma for the SRFB in Fig. 2, the zeros are the values of w so that if the base torque is $\tau(t) = e^{wt}$, the beam-end displacement and all of its time derivatives are zero; that is:

$$y(t,L_f) = (L_r + L_f)\theta + \xi(L_f,t) = 0 \tag{A14}$$

$$y^i(t,L_f) = 0 \tag{A15}$$

where $y^i(t,L_f) = d^i y(t,L_f)/dt^i$. From Eqs. (A12), (A14) and (A15), it can be concluded that the shear force and all its time derivatives are zero at the beam-end (note that the RHS of Eq. (A12) is the second time derivative of $y(t,L_f)$); that is:

$$EI\xi_{xxx}(L_f,t) = 0 \tag{A16}$$

$$EI\xi^i_{xxx}(L_f,t) = 0 \tag{A17}$$

where $EI\xi^i_{xxx}(L_f,t) = d^i(EI\xi_{xxx}(L_f,t))/dt^i$. Thus, for $\tau(t) = e^{wt}$, where w are the zeros of a SRFB, the following two properties hold:

(1) it appears that the beam is pinned at the beam-end; that is Eqs. (A14) and (A15) are satisfied, and simultaneously
(2) the shear force at the beam-end and its time derivatives are zero; that is Eqs. (A16) and (A17) are satisfied.

Thus from properties (1) and (2) above, for $\tau(t) = e^{wt}$ where w are the zeros of a SRFB, it can be concluded that the shear force at the beam-end of the pinned-pinned counterpart of the SRFB is zero. Consequently, based on the above Lemma, the zeros of a SRFB, w, are indeed the zeros of the pinned-pinned counterpart of the SRFB when the shear force at the beam-end is considered as the output.